The Knee 26 (2019) 185–193

Contents lists available at ScienceDirect

The Knee

Three-dimensional assessment of lower limb alignment: Accuracy and reliability

J. Fürmetz [a,*], J. Sass [a], T. Ferreira [b,c], J. Jalali [b], L. Kovacs [b], F. Mück [d], N. Degen [a], P.H. Thaller [a]

[a] 3D-Surgery, Department of General, Trauma- and Reconstructive Surgery, University Hospital Munich LMU, Germany
[b] Research Group CAPS—Computer Aided Plastic Surgery, Department of Plastic Surgery and Hand Surgery, University Hospital Klinikum rechts der Isar, Technische Universität München, Germany
[c] Faculty of Sciences, University of Lisbon, Portugal
[d] Department of Radiology, University Hospital Munich LMU, Germany

ARTICLE INFO

Article history:
Received 12 June 2018
Received in revised form 29 July 2018
Accepted 24 October 2018

Keywords:
3D anatomy
3D bone modeling
Alignment
Computed tomography
Patient-specific implant
Pre-operative planning

ABSTRACT

Introduction: Three-dimensional (3D) surgical planning and patient-specific implants are becoming increasingly popular in orthopedics and trauma surgery. In contrast to the established and standardized alignment assessment on two-dimensional (2D) long standing radiographs (LSRs) there is neither a standardized nor a validated protocol for the analysis of 3D bone models of the lower limb. This study aimed to create a prerequisite for pre-operative planning.
Methods: According to 2D analysis and after meticulous research, 24 landmarks were defined on 3D bone models obtained from computed axial tomography (CT) scans for a 3D alignment assessment. Three observers with different experience levels performed the test three different times on three specimens. Intraobserver and interobserver variability of the landmarks and the intraclass correlation coefficient (ICC) of the resulting axes and joint angles were evaluated.
Results: Overall, the intraobserver and interobserver variability was low, with a mean deviation <5 mm for all landmarks. The ICC of all joint angles and axis deviations was >0.8, except for tibial torsion (ICC = 0.69). All knee joint angles showed excellent ICC (>0.95).
Conclusions: Using the defined landmarks, a standardized 3D alignment assessment with low intraobserver and interobserver variability and high ICC values for the knee joint angles can be performed regardless of examiner's experience. The described method serves as a reliable standardized protocol for a 3D malalignment test of the lower limb. Three-dimensional preoperative analysis might enhance understanding of deformities and lead to a new focus in surgical planning.

1. Introduction

Precise pre-operative planning is a prerequisite to deformity surgery and joint replacement. Successful surgery is dependent on accurate planning and appropriate surgical tactics. Assessment of alignment on long standing radiographs (LSR) is the initial step in many pre-operative planning methods in deformity surgery of the lower limb and knee joint replacement [1]. This leads to a detailed analysis of the joint angles and mechanical axis deviation (MAD) in the frontal plane. If this axis deviation diverges from

* Corresponding author at: 3D Surgery, Knee Surgery and Sports Traumatology, Department of General, Trauma and Reconstructive Surgery, University Hospital Munich, Nußbaumstr, 20, 80336 München, Germany.
E-mail address: julian.fuermetz@med.uni-muenchen.de (J. Fürmetz).

https://doi.org/10.1016/j.knee.2018.10.011
0968-0160/

the physiological range (8 ± 7 mm medial to the knee joint center) it is considered to be a pathological malalignment [2]; however, rotation and knee flexion affect measurement of lower limb alignment. Therefore, pre-operative planning on LSR can be prone to error [3–5].

Despite the availability of three-dimensional (3D) imaging of bones obtained from computed axial tomography (CT), magnetic resonance imaging (MRI) or EOS imaging, surgical planning is still commonly performed on two-dimensional (2D) radiographs. However, due to technical progress in imaging procedures, 3D bone models and patient-specific cutting guides are increasingly popular in orthopedic surgery [6–9]. In total knee replacement, the manufacturing companies heavily promote these cutting guides and individualized implants. In deformity surgery, patient-specific cutting guides already exist for osteotomies around the knee and have shown promising results [6,10].

Detailed information regarding the 3D assessment of lower limb geometry is missing in both knee replacement and deformity surgery. Protocols for analyzing a computerized 3D bone model for mechanical alignment do exist, specifically for CT scans of the complete lower limb, CT scans of the joints (hip, knee and ankle), MRI and EOS imaging [4,11–16]. However, further aspects like malrotation/torsion and sagittal deformities are missed in the mentioned publications. It is believed that there is no standardized assessment of all these parameters in one testing protocol.

In order to work with patient-specific cutting guides and individualized implants around the knee, a standardized pre-operative 3D analysis equivalent to the assessment of alignment on LSR, the malalignment test described by Paley and Tetsworth, is necessary [1]. Due to the complex anatomy of 3D bone models, an assessment tool is needed that is simple, reliable and suitable for clinical use. All planes of possible deformities (coronal, sagittal and axial) have to be included in the 3D assessment of lower limb alignment.

This study aimed to close this gap and develop a standardized protocol for measuring lower limb anatomy on 3D bone models, and to determine interobserver and intraobserver variability. Therefore, existing work on 3D geometry and knowledge of 2D assessment were brought together in order to manually define bony landmarks with resulting axes and angles. It was hypothesized that by an exact point definition and standardized procedure a reliable 3D assessment of leg alignment would be possible independent of the experience of the examiner. In this study, accuracy and reliability were manually tested in order to provide a basis for comparison in future work with automatic point registration that is technically possible today.

2. Materials and methods

For this study, existing CT data of the lower limb of three different deceased patients was anonymized and segmented to create digital 3D bone models. The patients, of whom two were male and one female, ranged between 16 and 75 years. All of them were of Caucasian descent. Exclusion criteria included advanced osteoarthritis of the hip joint and knee joint, radiographic evidence of previous realignment surgery, fractures, or any lower extremity joint replacement. Institutional Review Board approval was obtained for the study (General Electric, Boston, USA).

The CT scans were all performed on a GE HD750 CT. The patients were positioned head first and scanned cranial to caudal with standardized CT parameters (helical acquisition, 120 kV, 0.8 s/rotation, 0.984:1 pitch factor, Scan field of view (SFOV) large body, dose modulation AutomA 100–650 mA with Noise Index 8.84). After data acquisition images were standardized, they were reconstructed in 1.25-mm slice thickness and intervals in bone kernel.

Concerning segmentation, the software Mimics 14.0 (Materialize, Leuven, Belgium) was used; more specifically, to first segment the CT images and subsequently calculate the 3D models. Following this, a 3D geometry of the leg including the femur, tibia, fibula, and patella with preserved spatial relationship was created. Finally, the surface of the bones was smoothed, and any small holes, tunnels or peaks on the surface were removed using the Geomagic Studio 2014 (3D Systems, Morrisville, NC, USA) software.

The generated 3D models were rotated and transformed in a new coordinate system in which the patella was centrally aligned between the femoral epicondyles in the new x–y plane. A centralized position of the patella is also common on conventional LSR. The x, y and z-axes are along the right–left, anterior–posterior and longitudinal axis, respectively.

Three observers participated in this study: an orthopedic surgeon (JF), a medical student (JS) and a bioengineer (TF). Two experienced surgeons (JF, PHT) defined relevant bony landmarks for the 3D assessment of alignment.

Previous work on bony anatomy, both 2D and 3D, helped the surgeons to determine these points [2,11–13,17,18]. The center of the femoral head and the center of the tibial articular surface of the ankle joint were chosen to define the mechanical axis [2,4,13]. The tip of the trochanter and the center of the neck shaft further described the proximal anatomy of the femur (neck shaft angle (NSA), lateral proximal femoral angle (LPFA), medial proximal femoral angle (MPFA)) [2,5,12]. The anatomical axes were determined by the midpoints of the femoral and tibial shaft at the level of one and two thirds of the shaft length [2,12]. The most distal points of the femoral condyles and the most proximal lateral and medial points of the tibia are necessary to describe the anatomical and mechanical distal femoral angle and proximal tibial angle (mLDFA, mPTA) [2,4,12]. Femoral torsion can be obtained as the angle between the line from the midpoint of the neck shaft to femoral head and the line built by the two most dorsal points of the femoral condyles. The tibial torsion is defined by the two most dorsal proximal points of the tibia and the two outermost points at the height of the ankle joint (medial and lateral malleolus) [19]. The medial and lateral tibial slope can be identified by the two lines between the most proximal anterior and posterior points and the anatomical tibial axis [2]. According to the study by Moreland et al. the current study utilized the center of the femoral trochlea (notch) as the femoral center of the knee and the center between the tibial spines on the tibial surface as the tibial center of knee [20]. The femoral and tibial knee centers define the mechanical axis of the femur and the tibia together with the center of the femoral head and the center of the tibial articular surface of the ankle [2,12]. Tables 1 and 2 and Figures 1 and 2 provide detailed descriptions of the bony landmarks, axes and angles.

This study aimed to design a standardized 3D assessment of the lower limb. Prior to the study, all observers were provided with specific instructions on point definitions as well as the means to find those (Table 1). Finally, each of the 24 landmarks of the lower limb was determined three times by three different observers with downtime of at least 1 week to reduce significant

Table 1
Definition of bony landmarks.

Bony landmark	Definition	Procedure to pinpoint
Femur		
Femoral hip center (FHC)	Midpoint of femoral head mass	Dorsal and ventral view[a,b] to create connected midpoints on both areas of the femoral head, medial view[c] to create midpoint on connecting line
Femoral neck center (FNC)	Midpoint of femoral neck mass	Dorsal and ventral view[a,b] to create connected midpoints on both areas of the femoral neck, medial view[c] to create midpoint on connecting line
Tip of greater trochanter (TGT)	Most cranial point (*y*-axis) on the greater trochanter	Dorsal view[a] to place, and lateral view[d] to confirm point
Femoral lateral condyle posterior (FLCP)	Most dorsal point (*z*-axis) on the lateral condyle	Caudal view[e] to place, and lateral view[d] to confirm point
Femoral medial condyle posterior (FMCP)	Most dorsal point (*z*-axis) on the medial condyle	Caudal view[e] to place, and medial view[c] to confirm point
Femoral lateral condyle distal (FLCD)	Most caudal point (*y*-axis) on the lateral condyle	Dorsal view[a] to place, and lateral view[d] to confirm point
Femoral medial condyle distal (FMCD)	Most caudal point (*y*-axis) on the medial condyle	Dorsal view[a] to place, and medial view[c] to confirm point
Femoral notch point (FNP)	Most cranial point (*y*-axis) of the femoral notch	Dorsal view[a] to place, and confirm point
Femoral anatomical axis proximal (FAAP)	Midpoint 1/3 down the femoral shaft	Dorsal and ventral view[a,b] to create connected midpoints on both areas of the femur, dividing it at the 1/3 mark (cranial ➔ caudal) into a cranial (1/3) and caudal (2/3) section, medial view[c] to create midpoint on connecting line
Femoral anatomical axis distal (FADP)	Midpoint 2/3 down the femoral shaft	Dorsal and ventral view[a,b] to create connected midpoints on both areas of the femur, dividing it at the 1/3 mark (caudal ➔ cranial) into a mid (1/3) and caudal (1/3) section, medial view[c] to create midpoint on connecting line
Tibia		
Tibial knee center (TKC)	Midpoint of the medial and lateral intercondylar tubercle	Dorsal view[a] to place, and cranial view[f] to confirm point
Tibial medial intercondylar tubercle (TMIT)	Most cranial point (*y*-axis) of the medial intercondylar tubercle	Dorsal view[a] to place and medial view[c] to confirm point
Tibial lateral intercondylar tubercle (TLIT)	Most cranial point (*y*-axis) of the lateral intercondylar tubercle	Dorsal view[a] to place and lateral view[d] to confirm point
Tibial medial condyle posterior (TMCP)	Most dorsal and cranial point (*z*-/*y*-axis) on the medial condyle	Cranial view[f] to place and dorsal view[a] to confirm point
Tibial lateral condyle posterior (TLCP)	Most dorsal and cranial point (*z*-/*y*-axis) on the lateral condyle	Cranial view[f] to place and dorsal view[a] to confirm point
Tibial medial condyle anterior (TMCA)	Most ventral and cranial point (*z*-/*y*-axis) on the medial condyle	Cranial view[f] to place and ventral view[b] to confirm point
Tibial lateral condyle anterior (TLCA)	Most ventral and cranial point (*z*-/*y*-axis) on the lateral condyle	crAnial view[f] to place and ventral view[b] to confirm point
Tibial medial condyle medial (TMCM)	Most medial and cranial point (*x*-/*z*-axis) on the medial condyle	Cranial view[f] to place and medial view[c] to confirm point
Tibial lateral condyle lateral (TLCL)	Most medial and cranial point (*x*-/*z*-axis) on the lateral condyle	Cranial view[f] to place and lateral view[d] to confirm point
Tibial ankle center (TAC)	Midpoint of the tibial plafond area	Caudal view[e] to place and confirm point
Tibial medial malleolus (TMM)	Most medial point of the medial malleolus	Caudal view[e] to place and medial view[c] to confirm point, avoid dorsal/ventral view[a,b] due to them being misleading because of the rotation
Tibial anatomical axis proximal (TAAP)	Midpoint 1/3 down the tibial shaft	Dorsal and ventral view[a,b] to create connected Midpoints on both areas of the tibia, dividing it at the 1/3 mark (cranial ➔ caudal) into a cranial (1/3) and caudal (2/3) section, medial view[c] to create midpoint on connecting line
Tibial anatomical axis distal (TADP)	Midpoint 2/3 down the tibial shaft	Dorsal and ventral view[a,b] to create connected midpoints on both areas of the tibia, dividing it at the 1/3 mark (caudal ➔ cranial) into a mid (1/3) and caudal (1/3) section, medial view[c] to create midpoint on connecting line
Fibula		
Fibular lateral malleolus (FLM)	Most lateral point of the lateral malleolus	Caudal view[e] to place and lateral view[d] to confirm point, avoid dorsal/ventral view[a,b] due to them being misleading because of the rotation

Detailed definition of 24 bony landmarks with description of how to place them on the 3D bone models.
[a] Dorsal view: looking at the backside
[b] Ventral view: looking at the frontside
[c] Medial view: looking at the left side of the right leg/right side of the left leg
[d] Lateral view: looking at the right side of the right leg/left side of the left leg
[e] Caudal view: looking from below to see the underside of the bone
[f] Cranial view: looking from above to see the top side

Table 2
Definition of axes, angles and mechanical axis deviation (MAD).

Axes and angles	Definition
Mikulicz line (ML):	FHC-TAC
Mechanical femoral axis (MFA):	FHC-FNP
Mechanical tibial axis (MTA):	TKC-TAC
Anatomical femoral axis (AFA):	FAAP-FADP
Anatomical tibial axis:	TAAP-TADP
Mechanical axis deviation total (MADt) (mm, %):	Minimal distance from ML to TKC
Mechanical axis deviation frontal (MADf) (mm, %):	Minimal deviation from ML to TKC in the *x*-axis
Mechanical axis deviation sagittal (MADs):	Minimal deviation from ML to TKC in the *y*-axis
Hip knee angle (HKA) (°):	Angle between MFA and MTA
Neck shaft angle (NSA) (°):	Angle between AFA and the axis FHC-FNC
Medial proximal femoral angle (MPFA) (°):	Angle between AFA and the axis FHC-TGT
Mechanical lateral distal femoral angle (mLDFA) (°):	Angle between MFA and the axis FLCD-FMCD
Medial proximal tibial angle (MPTA) (°):	Angle between MTA and the axis TLCL-TMCM
Joint line convergence angle (JLCA) (°):	Angle between the axes FLCD-FMCD and TLCL-TMCM in anteroposterior view
Medial tibial slope (°):	Angle between MTA and the axis TMCA-TMCP
Lateral tibial slope (°):	Angle between MTA and the axis TLCA-TLCP
Femoral torsion (°):	Angle between the axis FHC-FNC and FLCP-FMCP
Tibial torsion (°):	Angle between the axis TLCP-TMCP and TLM-TMM

memorization bias. The time to complete one leg was measured for each run. As a result of analyzing six lower limbs on three different specimens, for each of the 24 landmarks, a total of 54 ($6 \times 3 \times 3$) sets of coordinates was obtained.

Intraobserver and interobserver variability was defined as the distance between the mean position of a landmark to the observed position of the landmark [21]. For intraobserver precision, the mean positions of the landmarks P (x, y, z) and the distances (Di) to that mean position were calculated [11]. Intraobserver variability for each specific landmark was expressed by the mean value and standard deviation of Di. Interobserver precision was calculated using the mean coordinates found by each observer. Mean values, as well as standard deviation of the distances (Di) to these means, express the interobserver variability of that landmark [11].

Python scripting was used in Geomagic Studio 2014 to implement routine automation of the vector calculations. Using the coordinates of the landmarks the following formula was adapted to calculate vectors and angles:

$$\varphi = \cos^{-1}\left(\frac{\overrightarrow{v1} \times \overrightarrow{v2}}{|v_1| \times |v_2|}\right) \times \frac{360}{2\pi}$$

The intraobserver and interobserver variation of the femoral and tibial axes and all angles were based on the mean deviation of the bony landmarks. The variation was assumed to be random; therefore, simple error propagation estimations were used. For the angles, distances and MAD, the ICC was evaluated taking into account the multiple measurements by different observers on different specimens [21–23]. A two-way random effects model was used [23]. An ICC > 0.75 indicates good agreement [24]. mean values, maximum values, and standard deviations were obtained for all recorded distances and angles. The acquired data were summarized in Excel (Microsoft, USA) and statistically analyzed using SPSS version 20 (SPSS, Chicago, IL, USA).

3. Results

The intraobserver and interobserver variabilities concerning each landmark are displayed in Figures 2–4 and Tables 3 and 4. Mean deviations of all landmarks to the mean value were <5 mm, indicating overall acceptable agreement.

Mean intraobserver variability ranged from 0.6–4.6 mm. Interobserver variability had a similar range of 0.8–4.2 mm (Table 3). Variability was the highest for the most distal points of the femoral condyles (FMCD and FLCD) and for the medial and lateral malleolus (TMM and TLM) (Figures 2–4). The FLCD was responsible for the highest overall values in both interobserver and intraobserver variability. The resulting angular variation between axes was calculated based on the variability of the defined landmarks (see Tables 1 and 2). The mechanical axes of both femur and tibia could be very accurately determined due to the long distance between the defining points. Furthermore, the variability of the most distal points of the femoral condyles was shown to be high only in the axial plane, whereas such deviations could not be found in the frontal plane, therefore not affecting the mLDFA in any significant manner. Variability of tibial defining points for the mechanical axis was comparably low. All measured ICCs were > 0.75, except the tibial torsion, nonetheless showing a high overall correlation of all the measurements (Table 5). Differences in tibial torsion can be mostly attributed to the aforementioned higher variability in the landmarks of the lateral and medial malleolus. The average time measured to identify and verify all points on one leg was 17.22 min (SD 4.0) (range 9.50–27.44).

Figure 1. Transparent 3D bone model with relevant bony landmarks and mechanical femoral and tibial axes and Mikulizc line. Left anteroposterior view with femoral and tibial knee joint line; right sagittal view (for detailed description see Tables 1 and 2).

4. Discussion

This study focused on the 3D anatomy of the entire lower extremity. Although protocols to describe the anatomy of 3D bone models already exist, none of them are intended to serve as pre-operative analysis, the step before actual pre-operative surgical planning. Previous work on 3D alignment has mainly focused on different regions of the lower extremity (e.g. the knee) or specific aspects (e.g. coronal alignment), and leave maltorsion or sagittal deformities unaddressed [4,11,12,25].

The current results indicate a low intraobserver and interobserver variability of most defining landmarks on the bony anatomy. The mean intraobserver and interobserver error for all landmarks was <5 mm. Intraobserver reliability was <2 mm for all points (Observers 2 and 3). However, certain bony landmarks (FMCD, FLCD, TMM, TLM) showed much higher inter-rater and intra-rater variability than others, with high (TMM, TLM) and low (FMCD, FLCD) impacts on the resulting angles. Since FMCD and FLCD are placed on the surface of the distal femoral condyle, and therefore define the femoral knee joint line, deviations in the *x*-axis do not result in high angular differences. In contrast to this lateral and medial malleolus (TMM, TLM) highly affect the tibial torsion and variability of these points result in different angles, which is evidently reflected by the lower ICC (0.69) of tibial torsion. Manual setting of these landmarks seems to be prone to error, and may require computational automated setting of the landmarks to solve this problem.

The most relevant joint angles for deformity and knee surgery (MPTA and mLDFA) showed the highest agreement in both intra-rater and inter-rater variability as well as ICC (0.98 and 0.99). Compared to other work concerning 3D bony anatomy of

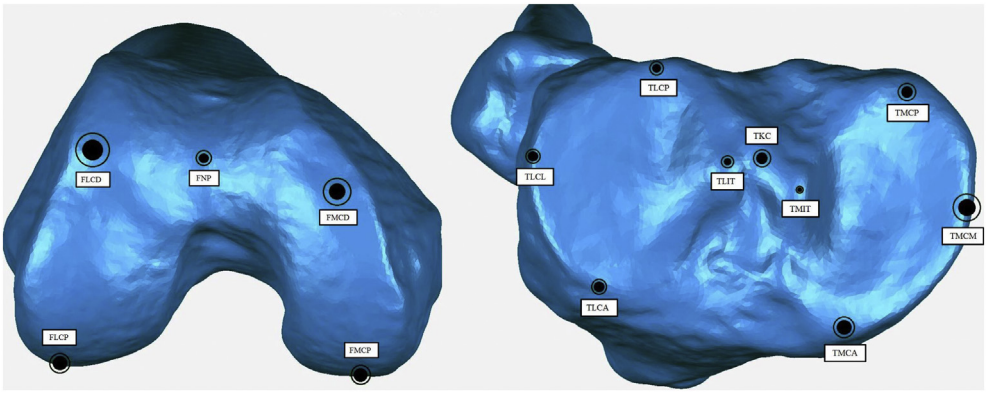

Figure 2. Bony landmarks of the distal femur (view caudal to cranial, left) and the proximal tibia (view cranial to caudal, right) on the 3D model. Black areas indicate the mean error and black thin circles indicate the mean error + 1 standard deviation. FLCD (Femoral lateral condyle distal), FMCD (Femoral medial condyle distal), FLCP (Femoral lateral condyle posterior), FMCP (Femoral medial condyle posterior), FNP (Femoral notch point), TLCL (Tibial lateral condyle lateral), TMCM (Tibial medial condyle medial), TLIT (Tibial lateral intercondylar tubercle), TMIT (Tibial medial intercondylar tubercle), TKC (Tibial knee center), TLCA (Tibial lateral condyle anterior), TLCP (Tibial lateral condyle posterior), TMCA (Tibial medial condyle anterior), TMCP (Tibial medial condyle posterior).

the knee, the variability in the current study was slightly elevated. This might be attributed to a broader focus, as opposed to analyzing one joint alone [11]. Another factor that might have influenced the variability could be the different levels of experience of the three observers.

Defining landmarks is a crucial step in developing a new method for analyzing 3D bony anatomy. Existing work on 3D anatomy of the lower limb and the knee was taken into consideration and therefore influenced the current definitions [4,11–13]. In addition, previously accepted knowledge about the 2D alignment on LSR and the assessment of lower limb torsion using CT was included [1,2,17,19,26–28]. Certain bony landmarks have a clear 3D definition, even when approached using different settings or techniques. When describing 3D anatomy, most authors use the method of a best fitting sphere to define the femoral hip center (FHC) [11–13]. As the current study focused on manual testing without computational calculations with regard to landmarks, two opposing points on the femoral head were defined to establish the corresponding center. This technique was also used for defining the center of the neck shaft at its lowest diameter, and for the centers of the femoral and tibial shafts. The automatic computer-aided calculation of these points (FHC, FNC, FAAC, FADC, TAAC, TADC) is not technically difficult and can probably significantly improve variability in future work.

Another crucial point in assessing the anatomy of the lower limb is the knee center. Moreland et al. defined five different points to describe the midpoint of the knee [20]. These points (center of the femoral notch, center of the femoral condyles, center of the tibial spines, center of soft tissue, and center of the tibial plateau) are all located within 5 mm on an LSR [2,20]. To define the extent of femoral and tibial contributions to the overall alignment, several authors have recommend a tibial and femoral knee center to separately define the mechanical axis of each bone [12,17,29]. Similar to other 3D studies, the notch was chosen as the femoral knee center based on the high consistency of that bony landmark [4,25]. As for the tibia, the midpoint of both tibial spines projected on the tibial surface represents the tibial knee center. Inter-rater and intra-rater reliability of HKA measurements on LSR using the center of tibial spines as the knee center had the best results [27]. Also, reliability of multiple measurements of this point is high in a 3D model [11]. Because of the favorable location on the bone surfaces, both tibial and femoral knee center

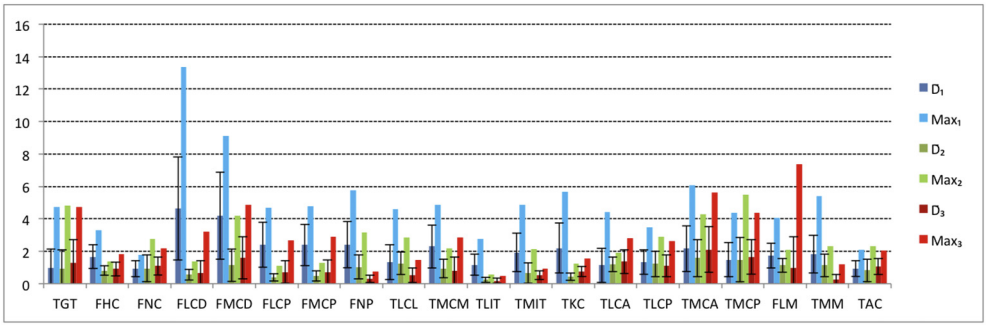

Figure 3. Intraobserver variability in the registration of bony landmarks. Mean values (mm) of all three observers (D1–3) with standard deviations and maximum values (Max 1–3) are displayed. TGT (Tip of greater trochanter), FHC (Femoral hip center), FNC (Femoral neck center), FLCD (Femoral lateral condyle distal), FMCD (Femoral medial condyle distal), FLCP (Femoral lateral condyle posterior), FMCP (Femoral medial condyle posterior), FNP (Femoral notch point), TLCL (Tibial lateral condyle lateral), TMCM (Tibial medial condyle medial), TLIT (Tibial lateral intercondylar tubercle), TMIT (Tibial medial intercondylar tubercle), TKC (Tibial knee center), TLCA (Tibial lateral condyle anterior), TLCP (Tibial lateral condyle posterior), TMCA (Tibial medial condyle anterior), TMCP (Tibial medial condyle posterior), FLM (Fibular lateral malleolus), TMM (Tibial medial malleolus), TAC (Tibial ankle center).

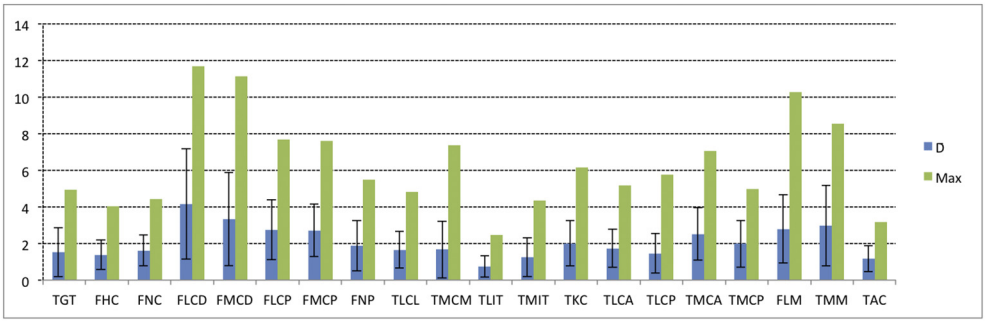

Figure 4. Interobserver variability in the registration of bony landmarks. Mean values (mm) (blue) with standard deviations and maximum values (green) are displayed. TGT (Tip of greater trochanter), FHC (Femoral hip center), FNC (Femoral neck center), FLCD (Femoral lateral condyle distal), FMCD (Femoral medial condyle distal), FLCP (Femoral lateral condyle posterior), FMCP (Femoral medial condyle posterior), FNP (Femoral notch point), TLCL (Tibial lateral condyle lateral), TMCM (Tibial medial condyle medial), TLIT (Tibial lateral intercondylar tubercle), TMIT (Tibial medial intercondylar tubercle), TKC (Tibial knee center), TLCA (Tibial lateral condyle anterior), TLCP (Tibial lateral condyle posterior), TMCA (Tibial medial condyle anterior), TMCP (Tibial medial condyle posterior), FLM (Fibular lateral malleolus), TMM (Tibial medial malleolus), TAC (Tibial ankle center).

can be easily displayed on a 3D reconstruction. It is important to clarify that these points must not be confounded with the rotational or biomechanical knee centers, as those change during normal gait.

Despite optimal circumstances for segmentation, creating the bone models and landmark registration in a controlled non-clinical setting, some of the defined landmarks still show a high variability, which is a clear limitation of the current study. An imaging technique with slice thickness of 1.25 mm in the main areas of interest seems not optimal for this testing protocol. In the regions of greatest interest (knee joint) a higher resolution (e.g. 0.625 mm slice thickness) could improve results whereas the shaft regions are not of such interest (e.g. 5 mm slice thickness). Improved protocols regarding CT scans and MRI should be developed for 3D anatomy assessment. Definitions of the mentioned landmarks with elevated variability should be further optimized to obtain a lower variability.

In conclusion, there is yet no set of landmarks universally accepted by experts when it comes to defining the 3D anatomy of the lower limb. Landmarks have to be both robust and clinically relevant. The presented landmarks have proven their reproducibility in standardized manual testing, but still leave room for future improvements, for example by means of automated point registration. Furthermore, more landmarks can be added to this 3D malalignment test in order to describe patellofemoral

Table 3
Interobserver and intraobserver variability of all landmarks.

	Interobserver deviation, mm	Intraobserver deviation, mm		
		1. Observer	2. Observer	3. Observer
	Mean (SD)	Mean (SD)	Mean (SD)	Mean (SD)
Femur				
Tip of greater trochanter (TGT)	**1.52** (1.34)	**0.98** (1.13)	**0.90** (1.18)	**1.27** (1.45)
Femoral hip center (FHC)	**1.39** (0.82)	**1.66** (0.72)	**0.80** (0.29)	**0.91** (0.43)
Femoral neck center (FNC)	**1.62** (0.84)	**0.92** (0.49)	**0.95** (0.82)	**1.09** (0.55)
Femoral lateral condyle distal (FLCD)	**4.17** (3.02)	**4.64** (3.19)	**0.56** (0.33)	**0.66** (0.77)
Femoral medial condyle distal (FMCD)	**3.33** (2.54)	**4.19** (2.68)	**1.13** (0.99)	**1.59** (1.29)
Femoral lateral condyle posterior (FLCP)	**2.75** (1.63)	**2.38** (1.38)	**0.39** (0.24)	**0.71** (0.69)
Femoral medial condyle posterior (FMCP)	**2.72** (1.45)	**2.39** (1.27)	**0.48** (0.32)	**0.72** (0.76)
Femoral notch point (FNP)	**1.87** (1.38)	**2.40** (1.42)	**1.03** (0.75)	**0.29** (0.22)
Tibia				
Tibial lateral condyle lateral (TLCL)	**1.66** (1.00)	**1.34** (1.08)	**1.26** (0.71)	**0.51** (0.44)
Tibial medial condyle lateral (TMCL)	**1.67** (1.55)	**2.30** (1.33)	**0.94** (0.57)	**0.77** (0.86)
Tibial medial intercondylar tubercle (TMIT)	**0.76** (0.59)	**1.17** (0.67)	**0.24** (0.16)	**0.18** (0.16)
Tibial lateral intercondylar tubercle (TLIT)	**1.25** (1.05)	**1.93** (1.20)	**0.64** (0.62)	**0.52** (0.28)
Tibial knee center (TKC)	**2.01** (1.24)	**2.20** (1.53)	**0.43** (0.24)	**0.76** (0.31)
Tibial lateral condyle anterior (TLCA)	**1.73** (1.04)	**1.14** (1.06)	**1.17** (0.45)	**1.37** (0.74)
Tibial lateral condyle posterior (TLCP)	**1.46** (1.08)	**1.33** (0.75)	**1.22** (0.80)	**1.09** (0.66)
Tibial medial condyle anterior (TMCA)	**2.52** (1.43)	**2.17** (1.41)	**1.58** (1.15)	**2.09** (1.41)
Tibial medial condyle posterior (TMCP)	**1.99** (1.28)	**1.47** (1.05)	**1.48** (1.36)	**1.64** (1.06)
Tibial medial malleolus (TMCM)	**2.97** (2.19)	**1.82** (1.16)	**1.13** (0.71)	**0.27** (0.30)
Tibial ankle center (TAC)	**1.17** (0.71)	**0.93** (0.48)	**0.82** (0.69)	**1.05** (0.50)
Fibula				
Fibular lateral malleolus (FLM)	**2.78** (1.86)	**1.73** (0.77)	**1.14** (0.43)	**0.98** (1.93)

Table 4
Mean values of all axes and angles. Mean values of the mechanical axis deviation (MAD).

		1. Observer	2. Observer	3. Observer
	Mean (SD)	Mean (SD)	Mean (SD)	Mean (SD)
Angles and axis (°)				
Tibial torsion	**27.11** (5.51)	**28.59** (5.64)	**29.19** (5.87)	**23.94** (2.91)
Medial tibial slope	**9.45** (2.38)	**8.64** (2.37)	**9.51** (2.27)	**9.97** (2.31)
Lateral tibial slope	**8.69** (1.92)	**8.47** (1.57)	**8.66** (1.65)	**8.86** (2.40)
Femoral torsion	**48.20** (4.57)	**46.01** (4.39)	**49.81** (4.15)	**48.40** (4.35)
LPFA	**89.91** (2.82)	**90.63** (3.53)	**90.16** (2.07)	**89.35** (2.51)
mLDFA	**86.58** (1.67)	**86.51** (1.56)	**86.61** (1.72)	**86.73** (1.71)
MPTA	**90.92** (1.40)	**90.95** (1.38)	**91.20** (1.36)	**90.63** (1.41)
MPFA	**96.24** (3.42)	**97.21** (4.12)	**96.42** (2.56)	**95.53** (3.19)
NSA	**129.73** (4.46)	**127.88** (4.90)	**131.10** (3.82)	**129.81** (3.96)
HKA	**175.97** (2.28)	**175.85** (2.45)	**176.21** (2.16)	**175.76** (2.19)
JLCA	**2.96** (2.12)	**2.62** (1.96)	**2.36** (2.12)	**2.95** (2.22)
MADF (%)	**43.70** (6.76)	**44.18** (6.63)	**43.96** (6.85)	**42.74** (6.72)
MADS (%)	**70.74**(32.08)	**71.93**(30.22)	**71.90** (33.50)	**69.40** (32.38)
MADT (mm)	**13.13** (7.15)	**13.52** (7.69)	**12.34** (6.71)	**13.86** (6.91)
MADF (mm)	**3.61** (5.12)	**3.15** (4.77)	**3.68** (5.23)	**4.30** (5.27)
MADS (mm)	**11.32** (7.49)	**12.06** (8.02)	**10.18** (7.27)	**12.03** (6.99)

LPFA (lateral proximal femoral angle), mLDFA (mechanical lateral distal femoral angle), MPTA (medial proximal tibial angle), MPFA (medial proximal femoral angle), NSA (neck shaft angle), HKA (hip knee angle), JLCA (joint line convergence angle), MADF (mechanical axis deviation frontal) (% of tibial width and mm), MADS (mechanical axis deviation sagittal) (% of tibial width and mm), MADT (mechanical axis deviation total).

pathologies, which will be an objective in future work. Additionally, a transfer of this malalignment test to 3D bone models obtained by MRI or EOS imaging with less radiation seems to be feasible.

5. Conclusion

A detailed standardized analysis of the 3D anatomy of the lower extremity was possible with a high degree of accuracy and reliability. This is the first step towards precise pre-operative planning in 3D of knee surgeries and deformity corrections of the lower limb.

Acknowledgements

The authors wish to thank Dipl.-Phys. Kirsi Manz and PD Dr. rer. biol. hum. Markus Pfirrmann (IBE – Institute for Medical Informatics, Biometry, and Epidemiology, Ludwig-Maximilians-Universität München) for their advice on the appropriate statistical methods used in this study. Further, we wish to thank Christina Lutz and James Schilling for their preliminary studies on this topic.

Table 5
Intraclass correlation (ICC) of relevant distances (MAD) and angles, indicating good agreement except tibial torsion.

	ICC	95% confidence interval
MAD total	0.98	0.937 < ICC < 0.998
MAD frontal	0.99	0.959 < ICC < 0.999
MAD sagittal	0.98	0.918 < ICC < 0.997
HKA frontal	0.96	0.942 < ICC < 0.998
HKA sagittal	0.99	0.942 < ICC < 0.998
NSA	0.94	0.488 < ICC < 0.992
MPFA	0.96	0.782 < ICC < 0.995
LPFA	0.96	0.799 < ICC < 0.994
mLDFA	0.99	0.968 < ICC < 0.999
MPTA	0.98	0.869 < ICC < 0.997
Medial slope	0.80	0.256 < ICC < 0.969
Lateral slope	0.90	0.583 < ICC < 0.985
Femoral torsion	0.92	0.410 < ICC < 0.990
Tibial torsion	0.69	0.040 < ICC < 0.950

MAD (mechanical axis deviation), HKA (hip knee angle), NSA (neck shaft angle), MPFA (medial proximal femoral angle), LPFA (lateral proximal femoral angle), mLDFA (mechanical lateral distal femoral angle), MPTA (medial proximal tibial angle).

Declarations of interest for all authors

None.

Funding

This research did not receive any specific grant from funding agencies in the public, commercial, or not-for-profit sectors.

References

[1] Paley D, Herzenberg JE, Tetsworth K, McKie J, Bhave A. Deformity planning for frontal and sagittal plane corrective osteotomies. Orthop Clin North Am 1994;25:425–65.
[2] Paley D. Principles of deformity correction. Springer: Berlin; 2005.
[3] Kawakami H, Sugano N, Yonenobu K, Yoshikawa H, Ochi T, Hattori A, Suzuki N. Effects of rotation on measurement of lower limb alignment for knee osteotomy. J Orthop Res 2004;22:1248–53. https://doi.org/10.1016/j.orthres.2004.03.016.
[4] Jamali AA, Meehan JP, Moroski NM, Anderson MJ, Lamba R, Parise C. Do small changes in rotation affect measurements of lower extremity limb alignment? J Orthop Surg 2017;12:77. https://doi.org/10.1186/s13018-017-0571-6.
[5] Degen N, Fürmetz J, Wolf F, Euler E, Thaller P. Medial proximal femoral angle better than neck-shaft angle? Influence of rotation on the anteroposterior radiograph. J Hip Surg 2017;01:146–51. https://doi.org/10.1055/s-0037-1607978.
[6] Victor J, Premanathan A. Virtual 3D planning and patient specific surgical guides for osteotomies around the knee: a feasibility and proof-of-concept study. Bone Joint J 2013;95-B:153–8. https://doi.org/10.1302/0301-620X.95B11.32950.
[7] Abane L, Anract P, Boisgard S, Descamps S, Courpied JP, Hamadouche M. A comparison of patient-specific and conventional instrumentation for total knee arthroplasty: a multicentre randomised controlled trial. Bone Joint J 2015;97-B:56–63. https://doi.org/10.1302/0301-620X.97B1.34440.
[8] Fürnstahl P, Vlachopoulos L, Schweizer A, Fucentese SF, Koch PP. Complex osteotomies of tibial plateau malunions using computer-assisted planning and patient-specific surgical guides. J Orthop Trauma 2015;29:e270–6. https://doi.org/10.1097/BOT.0000000000000301.
[9] Schotanus MG, Boonen B, Kort NP. Patient specific guides for total knee arthroplasty are ready for primetime. World J Orthop 2016;7:61–8. https://doi.org/10.5312/wjo.v7.i1.61.
[10] Arnal-Burró J, Pérez-Mañanes R, Gallo-Del-Valle E, Igualada-Blazquez C, Cuervas-Mons M, Vaquero-Martín J. Three dimensional-printed patient-specific cutting guides for femoral varization osteotomy: do it yourself. Knee 2017;24:1359–68. https://doi.org/10.1016/j.knee.2017.04.016.
[11] Victor J, Van Doninck D, Labey L, Innocenti B, Parizel PM, Bellemans J. How precise can bony landmarks be determined on a CT scan of the knee? Knee 2009;16:358–65. https://doi.org/10.1016/j.knee.2009.01.001.
[12] Subburaj K, Ravi B, Agarwal M. Computer-aided methods for assessing lower limb deformities in orthopaedic surgery planning. Comput Med Imaging Graph 2010;34:277–88. https://doi.org/10.1016/j.compmedimag.2009.11.003.
[13] Zheng G, Li S. Computational radiology for orthopaedic interventions. Berlin: Springer; 2015.
[14] Hinterwimmer S, Graichen H, Vogl TJ, Abolmaali N. An MRI-based technique for assessment of lower extremity deformities-reproducibility, accuracy, and clinical application. Eur Radiol 2008;18:1497–505. https://doi.org/10.1007/s00330-008-0896-y.
[15] Escott BG, Ravi B, Weathermon AC, Acharya J, Gordon CL, Babyn PS, et al. EOS low-dose radiography: a reliable and accurate upright assessment of lower-limb lengths. J Bone Joint Surg Am 2013;95:e1831–7. https://doi.org/10.2106/JBJS.L.00989.
[16] Meijer MF, Velleman T, Boerboom AL, Bulstra SK, Otten E, Stevens M, et al. The validity of a new low-dose Stereoradiography system to perform 2D and 3D knee prosthetic alignment measurements. PLoS One 2016;11:e0146187. https://doi.org/10.1371/journal.pone.0146187.
[17] Paley D, Tetsworth K. Mechanical axis deviation of the lower limbs: pre-operative planning of uniapical angular deformities of the tibia or femur. Clin Orthop 1992;280:48–64.
[18] Victor J, Glabbeek FV, Sloten JV, Parizel PM, Somville J, Bellemans J. An experimental model for kinematic analysis of the knee. J Bone Joint Surg Am 2009;91:150–63. https://doi.org/10.2106/JBJS.I.00498.
[19] Liodakis E, Doxastaki I, Chu K, Krettek C, Gaulke R, Citak M, et al. Reliability of the assessment of lower limb torsion using computed tomography: analysis of five different techniques. Skeletal Radiol 2012;41:305–11. https://doi.org/10.1007/s00256-011-1185-4.
[20] Moreland JR, Bassett LW, Hanker GJ. Radiographic analysis of the axial alignment of the lower extremity. J Bone Joint Surg Am 1987;69:745–9.
[21] Bland JM, Altman DG. Measurement error. BMJ 1996;312:1654.
[22] Rousson V, Gasser T, Seifert B. Assessing intrarater, interrater and test-retest reliability of continuous measurements. Stat Med 2002;21:3431–46. https://doi.org/10.1002/sim.1253.
[23] Shrout PE, Fleiss JL. Intraclass correlations: uses in assessing rater reliability. Psychol Bull 1979;86:420–8.
[24] Fleiss JL. The design and analysis of clinical experiments: fleiss/the design. Hoboken, NJ, USA: John Wiley & Sons, Inc.; 1999. https://doi.org/10.1002/9781118032923.
[25] Xing Q, Yang W, Theiss MM, Li J, Peng Q, Chen JX. 3D automatic feature construction system for lower limb alignment. IEEE 2010:375–82. https://doi.org/10.1109/CW.2010.15.
[26] Gordon JE, Chen RC, Dobbs MB, Luhmann SJ, Rich MM, Schoenecker PL. Interobserver and intraobserver reliability in the evaluation of mechanical axis deviation. J Pediatr Orthop 2009;29:281–4. https://doi.org/10.1097/BPO.0b013e31819b9188.
[27] McDaniel G, Mitchell KL, Charles C, Kraus VB. A comparison of five approaches to measurement of anatomic knee alignment from radiographs. Osteoarthr Cartil 2010;18:273–7. https://doi.org/10.1016/j.joca.2009.10.005.
[28] Strecker W, Keppler P, Gebhard F, Kinzl L. Length and torsion of the lower limb. J Bone Joint Surg Br 1997;79:1019–23.
[29] Cooke TDV, Sled EA, Scudamore RA. Frontal plane knee alignment: a call for standardized measurement. J Rheumatol 2007;34:1796–801.